Study of the glide elements in pyrite by means of electron microscopy and electron diffraction[1]

LUDO VAN GOETHEM, JOSEPH VAN LANDUYT AND SEVERIN AMELINCKX[2]

Rijksuniversitair Centrum Antwerpen (RUCA)
Middelheimlaan 1, B-2020 Antwerpen, Belgium

Abstract

The glide mechanism in pyrite was studied by electron microscopy and electron diffraction. Different configurations of antiphase boundaries and dislocations were analyzed by diffraction experiments. The antiphase boundaries lying in the cube plane could be described by a displacement vector $\frac{1}{2}[110]$ and they were terminated by dislocations for which a Burgers vector of the type $\frac{1}{2}[110]$ was deduced. At angular configurations of antiphase boundaries a stair–rod dislocation with Burgers vector $\frac{1}{2}[110]$ was observed.

A structural model is proposed for these defects. For the glide components we have found (100) $\frac{1}{2}[011]$, in variance with the NaCl system (110) $\frac{1}{2}[1\bar{1}0]$. This difference in behavior is explained in relation to structural aspects of pyrite.

Introduction

Pyrite has the NaCl structure where the sodium ions are replaced by iron and the chlorine ions by covalently bonded pairs of sulfur ions. These sulfur pairs are oriented along the $<111>$ directions of the smaller cubes in the unit cell (Wyckoff, 1965, p. 346). Due to the strong covalent bonding between the sulfur pairs these move as a whole during the glide; it is therefore of interest to study the differences between the glide mechanisms in NaCl and FeS_2. The glide elements in NaCl are known to be (110) $\frac{1}{2}[1\bar{1}0]$ (for a review see Haasen, 1974; Gilman and Johnston, 1962).

The glide elements were studied by means of an analysis of the dissociation of [110] dislocations into two partials terminating an APB between them. The glide plane was found to be the cube plane. The glide direction remains the same as for the NaCl structure.

Study of the glide mechanism

Specimen preparation

The specimens (pyrite single crystals from Logrono, Spain) were prepared in two different ways.

The first procedure can be summarized as follows:

three-mm discs were obtained from plates sawn perpendicular to [110]. These were further thinned by ion bombardment and electrochemical polishing. The electrolyte contained one part nitric acid in nine parts water. The voltage varied between 25 and 30 volts.

Another thinning procedure consisted in grinding the pyrite crystals under ethanol. A drop of the suspension thus obtained was deposited on a holey carbon grid. Specimens thinned in this way are submitted to important mechanical stresses.

Observations

Fringe pattern configurations (Fig. 1) were observed which are typical for translation faults. The patterns were terminated by dislocations in the case the defect ended in the foil. In the specimens prepared by electropolishing, these patterns usually extended over long distances in the foil and often they terminated at a grain boundary. These defects are probably due to growth. However, some isolated fringe patterns of shorter length (smaller than a few microns) were also observed. These terminated within the grains. The density of these shorter patterns in the ground specimens was much higher. They are most probably due to deformation, since by grinding the crystals are heavily deformed.

From contrast calculations using dynamical theory for electron diffraction, it follows that a translation interface, such as a stacking fault or an antiphase boundary, is imaged in the transmission electron mi-

croscope as a fringe pattern with a fringe periodicity related to the structure factor of the excited reflection. The contrast of the defects, which are characterised by a displacement vector $\bar{R}$ relating to the position of the two crystal parts with respect to each other, is determined by the phase factor $\alpha = 2\pi\bar{g}\cdot\bar{R}$ where the $\bar{g}$ denotes the active reflection. If $\alpha = 0$ or $2\pi n$ (n = integer) the contrast disappears and the translation interface is invisible or called out-of-contrast (for more information see Amelinckx and Van Landuyt, 1976). A dislocation is usually imaged as a dark line on a lighter background. Here the contrast is related to the vector product $\bar{g}\cdot\bar{b}$, where $\mathbf{b}$ is the Burgers vector of the dislocation. The invisibility criterion $\bar{g}\cdot\bar{b} = 0$ allows us to determine the Burgers vector from observation of the contrast for different $\bar{g}$ vectors.

Diffraction contrast analysis allowed us to interpret the fringe patterns as being associated with antiphase boundaries lying in a cube plane and having a displacement vector $\bar{R} = \frac{1}{2}[110]$ in the fault plane. The composition plane can be determined by tilting the specimen in such a way that the fault plane is oriented parallel to the electron beam. By relating the image and the diffraction pattern taken under these conditions the orientation of the fault plane can be obtained. A summary of the observed contrasts for some reflections is given in Table 1 for the displacement vectors $\bar{R} = \frac{1}{2}\langle 110\rangle$.

The two terminating dislocations always went si-

Table 1. Visibility of an antiphase boundary (APB) and a dislocation of the type encountered in pyrite as a function of the reflections $\bar{g}$ used for imaging in the two beam conditions (V: visible; I: invisible)

Reflection $\bar{g}$	APB $\bar{R} = \frac{1}{2}\langle 011\rangle$	dislocation $\bar{b} = \frac{1}{2}\langle 011\rangle$
(100)	I	I
(010)	V	V
(011)	I	V
(1$\bar{1}$1)	I	I
(021)	V	V
(001)	V	V
(11$\bar{1}$)	I	I

multaneously out of contrast for some of the reflections for which the antiphase boundary showed no contrast. This means that they have the same Burgers vector. It could be determined to be of the type $\bar{b} = \frac{1}{2}[110]$. The visibility conditions are also tabulated in Table 1. A model of the studied configuration is shown in Figure 2.

Angular configurations of antiphase boundaries were also observed, an example of which is shown in Figure 3. From the above-described tilting experiments it could be deduced that the plane of the antiphase boundary changed from one cube plane to another. The displacement vector for both orientations was again of the type $\bar{R} = \frac{1}{2}[110]$ with $\bar{R}$ lying in the respective planes [*e.g.* (100) $\frac{1}{2}\langle 011\rangle$, (010) $\frac{1}{2}\langle 10\bar{1}\rangle$]. At the bending edge a stair–rod dislocation is present with a Burgers vector which was also of the type $\frac{1}{2}[110]$.

Discussion

From the displacement vector for the faults as deduced by contrast experiments, and from the structural data for pyrite, we conclude that the antiphase boundaries can be described as interfaces between two crystal parts where the sulfur pairs have a different orientation. The Burgers vectors of the dislocations support a model whereby the configuration of antiphase boundaries limited by partial dislocations can result from the dissociation of a [110] dislocation into two $\frac{1}{2}[110]$ partials on a (001) glide plane. Since the dislocation energy is proportional to the square of the Burgers vector, this configuration causes a lowering of the energy, since the square of the Burgers vector of a [110] dislocation is larger than the sum of the squares of the Burgers vectors of the two partials. Another possible dissociation giving rise
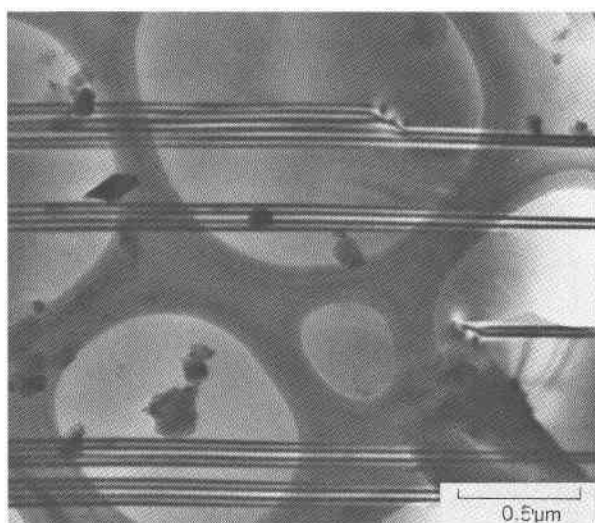

Fig. 1. Antiphase boundaries in pyrite. A typical π-fringe contrast is observed. Some antiphase boundaries end in the crystal and are terminated by a dislocation. The image shows a crystal fragment superposed on a holey carbon supporting film.
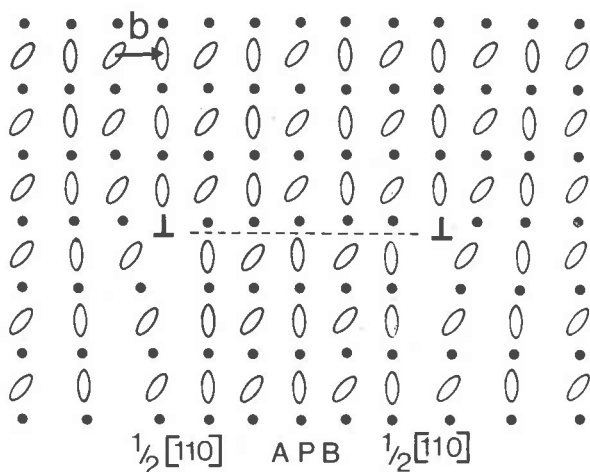
Fig. 2. Model for a dissociated [110] dislocation in a [1̄10] projection. Between the two ½[110] partials an antiphase boundary is present. The black dots (●) represent iron atoms, the open ellipses, sulfur pairs. Notice the change of the sulfur-pair orientation on crossing the boundary marked by a dashed line.

Fig. 3. Angular configuration of antiphase boundaries. The stair–rod dislocation is visible at the bending edge.

to an antiphase boundary with $\bar{\mathbf{R}} = \frac{1}{2}\langle 110 \rangle$ is:

$$\langle 100 \rangle \rightarrow \tfrac{1}{2}\langle 110 \rangle + \tfrac{1}{2}\langle 1\bar{1}0 \rangle$$

This dissociation does not decrease the energy, however, and consequently this mechanism of dissociation was not observed.

The angular configurations as shown in Figure 2 may result either from growth or glide on two planes since they occur in both kind of specimens. In the second kind they also occur in small isolated groups, while in the first kind the separate antiphase boundaries extend over longer distances. The Burgers vector of the stair–rod dislocation, being the sum of the displacement vectors of the two antiphase boundaries, can be $\frac{1}{2}[112]$ {e.g. the system (100) $\frac{1}{2}\langle 011 \rangle$, (010) $\frac{1}{2}\langle 101 \rangle$} or $\frac{1}{2}[110]$ {e.g. (100) $\frac{1}{2}\langle 011 \rangle$, (010) $\frac{1}{2}\langle 10\bar{1} \rangle$}. Only the second kind was observed, which is compatible with energy considerations. Moreover, the $\frac{1}{2}[112]$ dislocation has a larger energy than the $\frac{1}{2}[110]$ dislocation.

Whereas the Burgers vector $\frac{1}{2}[110]$ is a lattice vector for the NaCl structure, it is not for the structure of pyrite. This clearly results from the fact that whereas in NaCl all Cl ions are equivalent, this is no longer the case for the sulfur pairs. The repeat distance in the [110] direction is consequently doubled, and the pyrite structure can be considered as a superstructure of the NaCl structure. A structure fault is
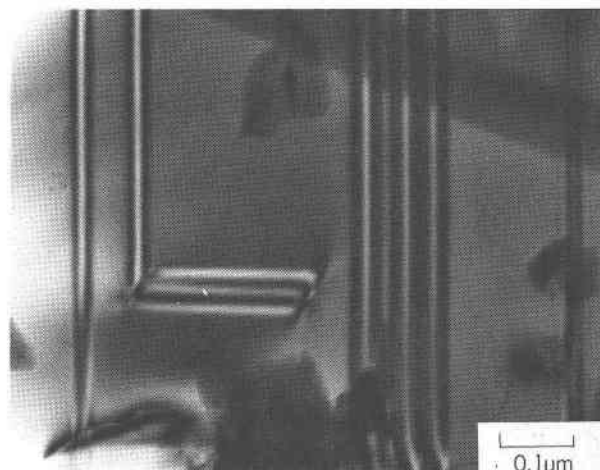
then expected between the two partial dislocations, which is evidenced by the fringe pattern connecting them (e.g. Fig.1).

We conclude from the observations that in pyrite the glide plane is the cube plane as compared to the (110) plane in NaCl, but the glide direction remains the same as in NaCl. Intuitively one can understand this as follows: In the [110] direction only atoms of one kind are present (model Fig.3). Whatever glide happens, the atomic sites remain occupied by the same type of atoms (Gilman and Johnston, 1962). This direction also corresponds to the valleys between the sulfur pairs if one goes from one iron atom to its nearest neighbor in a cube plane. The axis of all sulfur pairs makes the same angle with a cube plane (36°). In other possible glide planes this angle can become much larger for a fraction of the pairs. Consequently the {100} plane can be considered as the "smoothest" plane for the structure.

References

Amelinckx, S. and J. Van Landuyt (1976) Contrast effects at planar interfaces. In H. R. Wenk, Ed., Electron Microscopy in Mineralogy, p. 68–112. Springer-Verlag, Berlin.

Gilman, J. J. and W. G. Johnston (1962) Dislocations in LiF crystals. Solid State Phys., 13, 148–216.

Haasen, P. (1974) Dissociation of dislocations and plasticity of ionic crystals. J. Physique, 167–172.

Wyckoff, R. W. G. (1965) Crystal Structures, Vol. 1, 2nd ed., Wiley, New York.